Functionalized bismuth ferrite harmonic nanoparticles
for cancer cells labelling and imaging

Solène Passemard, Davide Staedler, Giona Sonego, Thibaud Magouroux, Guillaume Stéphane Schneiter, Lucienne Juillerat-Jeanneret, Luigi Bonacina, Sandrine Gerber-Lemaire

S. Passemard, D. Staedler, G. Sonego, G. S. Schneiter, S. Gerber-Lemaire (corresponding author)
Institute of Chemical Sciences and Engineering, Ecole Polytechnique Fédérale de Lausanne, Batochime, CH-1015 Lausanne, Switzerland
e-mail: Sandrine.Gerber@epfl.ch

T.Magouroux, L. Bonacina
GAP-Biophotonics, Université de Genève, 22 Chemin de Pinchat, 1211 Genève 4, Switzerland

L. Juillerat-Jeanneret
University Institute of Pathology, CHUV-UNIL, CH-1011, Lausanne, Switzerland

Abstract

Bismuth ferrite (BFO) harmonic nanoparticles (NPs) display high nonlinear optical efficiency and excellent biocompatibility profile which make them attractive for the development of diagnostic applications as contrast agents. In this study, we present a general method for the functionalization of this material with chemical ligands targeting cancer molecular biomarkers. In particular, a conjugation protocol based on click reaction between alkynyl containing targeting ligands and poly(ethylene glycol) coated BFO NPs (67.7 nm) displaying surface reactive azido groups was developed. Copper-free click reaction allowed fast and efficient conjugation of a covalent inhibitor of prolyl-specific endopeptidases to coated BFO NPs. The ability of these functionalized nanomaterials (134.2 nm) to act as imaging probes for cancer cells was demonstrated by the selective labelling of human lung cancer cells.

Keywords

Functionalized nanoparticles

Harmonic nanoparticles

Cancer cells targeting

Prolyl endopeptidase inhibitors

Electronic supplementary material

The online version of this article contains supplementary material, which is available to authorized users.

Introduction

Nanomaterials, and in particular nanoparticles (NPs), are being increasingly developed as contrast agents for the imaging of fundamental biological processes. Several types of materials, including silica NPs and nanocomposites (Wang et al. 2015), quantum dots (Kairdolf et al. 2013), carbonaceous nanomaterials (Wen et al. 2015), semiconductor nanotubes and nanosheets (Ahmad et al. 2015), upconversion and metal oxide NPs (Erathodiyil et al. 2011; Zhou et al. 2015) have been widely explored for bioimaging applications. While fluorescence/luminescence (Yao et al. 2014; Wolfbeis 2015; Chinen et al. ASAP) and plasmonic response (Bardhan et al. 2011) are the most common optical properties used for imaging techniques, nonlinear optical response has only been recently demonstrated in a series of promising imaging applications. In this context, harmonic nanoparticles (HNPs), which are composed by non-centrosymmetric materials presenting a highly efficient nonlinear response, can be easily imaged by their second harmonic generation signal in multi-photon imaging setups (Bonacina 2012; Cohen 2010; Pantazis et al. 2010; Meyer et al. 2013). In contrast with most nanophotonic probes for bioimaging applications which are based on static optical properties, HNPs can fully exploit the tuning capabilities offered by new laser sources (from 400 to 1550 nm). In addition, despite their lower brightness compared to fluorescence imaging labels, HNPs present many favorable properties for optical imaging, including the absence of photobleaching and blinking (Le Xuan et al. 2008), no specific wavelength dependence allowing excitation from UV to IR (Extermann et al. 2009), fully coherent response and narrow emission signals (Baumner et al. 2010; Hsieh et al. 2010). These unique features combined in a single optical probe have been recently reported for cell, tissue and *in vivo* imaging applications (Čulić-Viskota et al. 2012, Dempsey et al. 2012, Magouroux et al. 2012).

Various types of HNPs, mainly metal oxide materials, have been produced and characterized, such as barium titanate ($BaTiO_3$), iron iodate ($Fe(IO3)_3$), lithium niobate ($LiNbO_3$), potassium niobate ($KNbO_3$), potassium titanyl phosphate (KTP) and zinc oxide (ZnO). In a comprehensive study, we demonstrated that these nanoparticles display efficient harmonic conversion and low cytotoxicity with the exception of ZnO materials (Staedler et al. 2012). More recently, bismuth ferrite nanoparticles ($BiFeO_3$, abbreviated as BFO-NPs) were introduced as promising nonlinear optical probes due to their very high second harmonic efficiency which was demonstrated to be one order of magnitude higher than for standard harmonic nanomaterials (Schwung et al. 2014). In addition, we gave evidence for the good biocompatibility of PEGylated BFO-NPs (Staedler et al. 2015) and for the ability of BFO-NPs to locally induce

DNA damage by deep UV generation (Staedler et al. 2014). In view of the favorable profile of these HNPs for bio-imaging applications, their functionalization with targeting entities was envisaged for the development of nanoprobes for cancer cells labelling. Different types of targeting agents, including antibodies, peptides and small molecules have been conjugated to inorganic NPs for the detection of cancer molecular biomarkers. Antibodies offer high affinity and selectivity to the resulting conjugates, but may alter the permeability of NPs across the vasculature and the blood vessel walls as they considerably increase the size of the NPs (Arruebo et al. 2009). Antibody-NPs conjugates may also induce adverse immune response over prolonged use. Therefore, surface modification of BFO-NPs with low molecular weight targeting ligands appears as an appealing strategy for the detection of cancer cells (Sun et al. 2006).

We report herein a functionalization methodology for the conjugation of PEGylated BFO-NPs to cancer targeting ligands based on azide-alkyne [3+2] cycloaddition (click reaction), catalyzed by copper (I) species (Rostovtsev et al. 2002) or promoted by the use of strained cyclooctynes (Sletten et al. 2011). In particular, the cyclic Arg-Gly-Asp (RGD) peptide derivative cRGDfK, a ligand for the $\alpha_v\beta_3$ integrin (Danhier et al. 2012), and a specific inhibitor of prolyl-endopeptidases (Juillerat-Jeanneret et al. 2009; Brennen et al. 2012), respectively, were covalently associated to the nanoparticles surface for recognition of the cancer cells and cancer associated-cells membrane molecular biomarkers. The resulting cancer-targeting NPs have been characterized and evaluated for their ability to label human lung cancer cells.

Materials and methods

Chemical syntheses – General conditions

Commercial reagents (Fluka, Aldrich, TCI, Switzerland) were used without further purification. Unless special mention, all reactions were performed under argon atmosphere (1 atm). Anhydrous solvents were obtained by filtration (Innovative Technology, Oldham, UK). Reactions were monitored by TLC (Merck silica gel 60F254 plates, Merck, Darmstadt, Germany). Detection was performed by UV light, $KMnO_4$, Ninhydrin or I_2. Purifications were performed by flash chromatography on silica gel (Merck N° 9385 silica gel 60, 240-400 mesh). IR spectra were recorded on a Perkin-Elmer-1420 spectrometer (Perkin-Elmer, Waltham, MA, USA). ^{1}H-NMR spectra were recorded on a Bruker ARX-400 spectrometer (400 MHz) (Bruker, Billerica, MA, USA). ^{13}C-NMR spectra were recorded on a Bruker ARX-400 spectrometer

(100.6 MHz). Chemical shifts are expressed in parts per million (ppm) and coupling constants (*J*) in hertz. Solvents used for NMR spectroscopy are deuterated chloroform (CDCl$_3$, Acros) and deuterated methanol (CD$_3$OD, Acros). Mass spectra were obtained on a Nermag R-10-10C spectrometer with chemical ionization (NH$_3$) and mode m/z (amu) [% relative base peak (100%)] (Nermag, Santa Clara, CA, USA). Semi-preparative HPLC was performed on a Waters Autopurification ZQ System equipped with a 2767 Sample Manager, a 2525 Binary Gradient Module and a 2996 Photodiode Array Detector, coupled to Waters Micromass ZQ analyzer. The HPLC purifications were performed on XTerra Prep RP C18 (19 x 150 mm) columns, using reverse-phase conditions (2 to 100% acetonitrile with 0.1% TFA over 20 min). Measurements of the dynamic light scattering and zeta potential were obtained using a Malvern NanoZ instrument (Malvern Instruments, Malvern, UK).

Synthesis of targeting ligands (Scheme 2)

*Synthesis of tert-butyl [(3-oxo-1,2-dihydro-1H-isoindol-5-yl)oxy]acetate (**4**).*
To a solution of **3** (6.13 mmol, 1.0 g) in CH$_3$SO$_3$H (20 equiv, 7.96 mL) was added methionine (1.8 equiv, 11.04 mmol, 1.64 g) and the mixture was stirred at 85 °C for 16 h. After cooling to 25 °C, cold water (5 °C) was added, and the mixture was maintained at 5 °C for 1 h. The solid was recovered by filtration, washed with water containing aqueous 1% HCl, and then dried to afford the intermediate phenol (664 mg, 73 %) as a white solid. To a solution of this intermediate (11.4 mmol, 1.7 g) in *N*,*N*-dimethylformamide (DMF)/ dichloromethane (DCM) (1:1, 20 mL), were added *tert*-butyl bromoacetate (11.97 mmol, 3.11 g, 2.35 mL), Bu$_4$NBr (0.57 mmol, 184 mg) and 50 % aqueous NaOH (11.97 mmol, 479 mg). The mixture was stirred for 16 h at 25°C and the product was extracted with DCM (20 mL). The organic layer was dried (MgSO$_4$) and concentrated in vacuo. Purification by flash chromatography (petroleum ether (PE)/EtOAc 1:1) gave **4** as a white solid (1.88 g, 62 %). ESI-HRMS: calcd for C$_{14}$H$_{17}$NO$_4$: 264.1236; found: 264.1244. ^{1}H-, ^{13}C- NMR and IR spectral description are given in supporting information.

*Synthesis of (S)-tert-butyl 2-((2-(2-(2-cyanopyrrolidin-1-yl)-2-oxoethyl)-3-oxoisoindolin-5-yl)oxy)acetate (**6**).*
1M Lithium bis(trimethylsilyl)amide (LiHMDS) in tetrahydrofuran (THF) (615 µmol, 615 µL) was added to a cooled (0 °C) solution of **4** (410 µmol, 107 mg) in THF (1.2 mL). After 30 min, a solution of **5** (529 µmol, 115 mg) in THF (1.2 mL) was added dropwise. The mixture was

5

slowly warmed to 25°C and was stirred for 10 h. Completion of the reaction was monitored by thin-layer chromatography (TLC) and ESI-MS. Volatiles were removed in vacuo. The crude residue was purified by flash chromatography (DCM, then DCM/MeOH 60: 1) to afford **6** as a transparent oil (0.120 g, 73 %). ESI-HRMS: calcd for $C_{21}H_{25}N_3O_5$: 400.1873, found 400.1886. ^{1}H-, ^{13}C- NMR and IR spectral description are given in supporting information.

Synthesis of ligand 2

Compound **6** (1.25 mmol, 500 mg) was added to a suspension of silica (6.25 g) in toluene (25 mL). The mixture was refluxed for 1.5 h under vigorous stirring. The mixture was diluted in DCM/MeOH 4:1 and celite was added. The mixture was filtered. The pad of celite was washed with DCM/MeOH 4:1 and the combined filtrates were evaporated under reduced pressure to obtain free carboxylic acid intermediate as a white solid (quant.). To this compound (131 µmol, 45 mg) in DMF (1 mL) were added compound **7** (137 µmol, 60 mg), 1-ethyl-3-(3-dimethylaminopropyl)carbodiimide (EDCI) (222 µmol, 43 mg), 1-hydroxybenzotriazole (HOBt) (170.3 µmol, 23 mg) and (^{i}Pr)$_2$NEt (393 µmol, 50.8 mg, 65 µL). The reaction mixture was stirred for 12 h at 25 °C. DMF was evaporated and the product was purified by flash chromatography (DCM/MeOH 25:1) to afford **2** as a colorless oil (98 µmol, 75 mg, 75 %). ESI-HRMS: calcd. for $C_{42}H_{45}N_5O_9$: 764.3295; found: 764.3293. ^{1}H-, ^{13}C- NMR and IR spectral description are given in supporting information.

Functionalization of BFO-NPs (Scheme 3)

Functionalization of PEG-BFO NPs with ligand 1

To a suspension of PEG-BFO NPs (6 mg) in EtOH (1 mL) was added distilled water (2 mL) and **1** (4 mg, dissolved in 100 µL of DMF). $CuSO_4$ (2 mg) and sodium ascorbate (2 mg) were added and the suspension was ultra-sonicated for 12 h at 40 °C. 1,4,8,11-Tetraazacyclotetradecane (Cyclam) (10 mg) was added and the suspension was dialyzed against a solution of dodecyltrimethylammonium bromide in distilled water (0.1 M, 2 mL) for 24 h followed by dialysis against distilled water (3 x 24 h). **fNP-1** were concentrated and suspended in EtOH (1 mL).

Functionalization of PEG-BFO NPs with ligand 2

To a suspension of PEG-BFO NPs (5.5 mg) in EtOH (1 mL) were added distilled water (5 mL) and **2** (13 µmol, 10 mg, dissolved in 750 µL of DMF). The suspension was ultra-sonicated for

6

12 h at 40 °C. The suspension was washed with toluene (3 x 5 mL) and organic layers were washed with water. Combined aqueous layers were evaporated and co-evaporated with toluene in vacuo. The resulting **fNP-2** were suspended in EtOH (1 mL).

Characterization of functionalized BFO NPs: DLS and zeta potential measurement

A suspension of coated or functionalized NPs (20 µL) was diluted with distilled H_2O (1 mL) and AcOH (100 µL) was added. The resulting suspension was ultra-sonicated for 5 min and washed 3 times with distilled H_2O (1 mL). NPs were suspended in distilled water (1 mL) and sonicated for 30 min. The sizes and surface charges of the resulting suspensions were analyzed with a Malvern NanoZ instrument (Malvern Instruments, Malvern, UK).

Inhibition of human recombinant enzyme by compound **8**

The human recombinant enzymes were obtained from: hrDPPIV (Enzo Life Sciences, Lausen, Switzerland), hrFAPα (R&D systems, Abingdon, UK) and hrPOP/PREP (Enzo Life Sciences). The enzymatic activity was measured in flat bottom 96-well plates (Costar, Corning, NY, USA) containing in each well 0.01 µg of the enzymes and 50 µM of substrate (Z-Gly-Pro-AMC for hrFAPα and hrPOP, and H-Gly-Pro-AMC for hrDPPIV, both substrates from Bachem) diluted in their respective assay buffers (50 mM Tris, 1 M NaCl and 1 mg/mL bovin serum albumin (BSA), pH 7.5, for hrFAPα; 50 mM Tris and 1 mg/mL BSA, pH 7.5, for hrPOP; 25 mM Tris and 1 mg/mL BSA, pH 8.0 for hrDPPIV; all reagents from Sigma-Aldrich, Buchs, Switzerland). The enzyme solutions were incubated for 30 min with increasing concentrations (5, 10, 50, 200, 500, 1000, 5000 and 10000 nM) of compound **8**. Then inhibition was determined by evaluation of the residual enzymatic activity: measurement of the fluorescence increase for 1 h at 37°C in a fluorescence multi-well plate reader (λex/λem = 360/460 nm, Synergy HT, BioTek, Winooski, VT, USA). Experiments were conducted in triplicate wells and repeated twice. IC_{50} and K_i were calculated according to Cer et al (2009).

Cells and cell culture conditions

A549, BEAS-2B, NCI-H596, NCI-H520 cell lines are available from ATCC (American Tissue Culture Collection, Manassas, VA, USA). A549 and BEAS-2B cells were grown in Dulbecco's Modified Eagle Medium (DMEM) medium containing 4.5 g/L glucose, 10% heat-inactivated

fetal calf serum (FCS) and penicillin/streptomycin (all cell culture reagents were obtained from Invitrogen, Basel, Switzerland). NCI-H596 cells were grown in complete Roswell Park Memorial Institute (RPMI) 1640 medium (Invitrogen) supplemented with 20% FCS and penicillin/streptomycin. NCI-H520 cells were grown in RPMI 1640 medium supplemented with 10% FCS and penicillin/streptomycin.

Detection of the association of compound **8** with cells

The cells were grown for 48 h in BD Falcon CultureSlides (BD Biosciences, Erembodegem, Belgium), then the cell layers were washed with Hank's Balanced Salt Solution (HBSS) at 37 °C, exposed to 100 µM of compound **8** or to vehicle (dimethyl sulfoxide (DMSO)), 0.5% final concentration) in HBSS for 30 min at 37 °C. Cell layers were washed twice with HBSS and fixed with 4% formaldehyde in PBS for 30 min at 5 °C. The fixed cell layers were blocked for 1h with 1% BSA in PBS (phosphate buffered saline) at room temperature, then washed and exposed to horseradish peroxidase (HRP)-conjugated streptavidin (Merck) diluted 1:100 in antibody diluent (Dako, Baar, Switzerland). HRP activity was revealed using the DAB+ CHROMOGEN^{TM} system from Dako, according to the supplier instructions. Finally, the cell layers were counterstained with hematoxylin and images were taken using a transmitted light microscope (DM IL LED from Leica, Renens, Switzerland) equipped with a digital camera (ICC50HD, Leica).

Inhibition of prolyl-oligopeptidase activities in living cells

The cells (50'000 cells/well) were grown for 24 h in flat bottom 96 well plates (Corning), then were exposed to increasing concentrations (5, 10 and 20 µM) of compound **8** and to 50 µM of Z-Gly-Pro-7-amino-4-methylcoumarin (AMC) (for prolyl-endopeptidase activity) or 50 µM of H-Gly-Pro-AMC (for prolyl-exopeptidase activity) (Bachem, Vionnaz, Switzerland). Fluorescence increase was measured for 1 h at 37 °C in a fluorescence multi-well plate reader (Synergy HT) at λex/λem = 360/460 nm. Experiments were conducted in triplicate wells and repeated twice. Means $\pm$ standard deviations were calculated.

Detection of the association between compound **8** and cells

The cells were grown for 48 h in BD Falcon CultureSlides (BD Biosciences), then the cell layers were exposed to vehicle (DMSO) or to compound **8** at the indicated time and concentrations in cell medium at 37 °C. After the incubation time, the cell layers were fixed with 4% formaldehyde in PBS for 30 min at 5 °C. Fixed cells were then washed with PBS, permeabilized 5 min in 0.1% Triton X-100 (Sigma-Aldrich) in PBS, incubated 10 min at 25 °C in 3% H_2O_2 in methanol and blocked 2h with 1% BSA in PBS at 25 °C, then washed and exposed for 90 min to HRP-conjugated streptavidin (Merck) diluted 1:100 in antibody diluent (Dako). HRP activity was revealed using the DAB+ CHROMOGENTM system from Dako, according to the supplier instructions. Finally, the cells were counterstained with hematoxylin and images were taken using a transmitted light microscope (DM IL LED from Leica) equipped with a digital camera (ICC50HD, Leica).

Multiphoton imaging of the association between **fNP-2** and cells

Cells were grown on round-shaped microscope coverslips (BD Falcon) for 24 h in a 24 well plate (Corning) then the cell layers were washed with HBSS at 37 °C and exposed to the coated and functionalized NPs at indicated concentrations or to vehicle (ethanol, 1% final concentration) in 500 µL HBSS for indicated time at 37 °C. The cell layers were washed twice with HBSS and fixed in 4 % formaldehyde in PBS for 30 min at 5 °C. After fixation, the cells were labelled with fluorescent probes.

For imaging, a multiphoton inverted microscope (Nikon A1R-MP) coupled with a tunable Ti:Sapphire oscillator (Spectra-Physics Mai-Tai, 100 fs, 80 MHz, 700-1000 nm) was used. A 20× N.A. 0.75 objective was used to focus the excitation laser and to epi-collect the SHG signal from the nanoparticles and dye markers fluorescence. Typical average power at the sample: 3 mW.

Results and discussion

Efficient surface functionalization of BFO NPs is of high importance for bio-imaging applications, in particular for targeted imaging of cancer cells and early stage tumors. We decided to explore the conjugation of targeting entities by click reaction between PEGylated BFO NPs displaying surface reactive azido groups and alkynyl containing ligands designed for recognition of molecular cancer biomarkers (Scheme 1). $\alpha_v\beta_3$ Integrin is a well-established target for cancer diagnosis (Desgrosellier et al. 2010) and can be efficiently bound by cyclic

RGD peptides and RGD peptidomimetics. Prolyl-oligopeptidases, in particular the serine proteases FAPα which exhibits both exopeptidase and endoproteolytic activity, and prolyl-oligopeptidase (POP) which is restricted to endoproteolytic cleavages, have been associated with the development of cancers and other diseases (Brennen et al. 2012; Lawandi et al. 2010). Covalent inhibitors based on previously reported N-blocked boroPro inhibitors (Poplawski et al. 2013) can thus be developed for the labelling of malignant cells and tumor-associated cells expressing these enzymes.
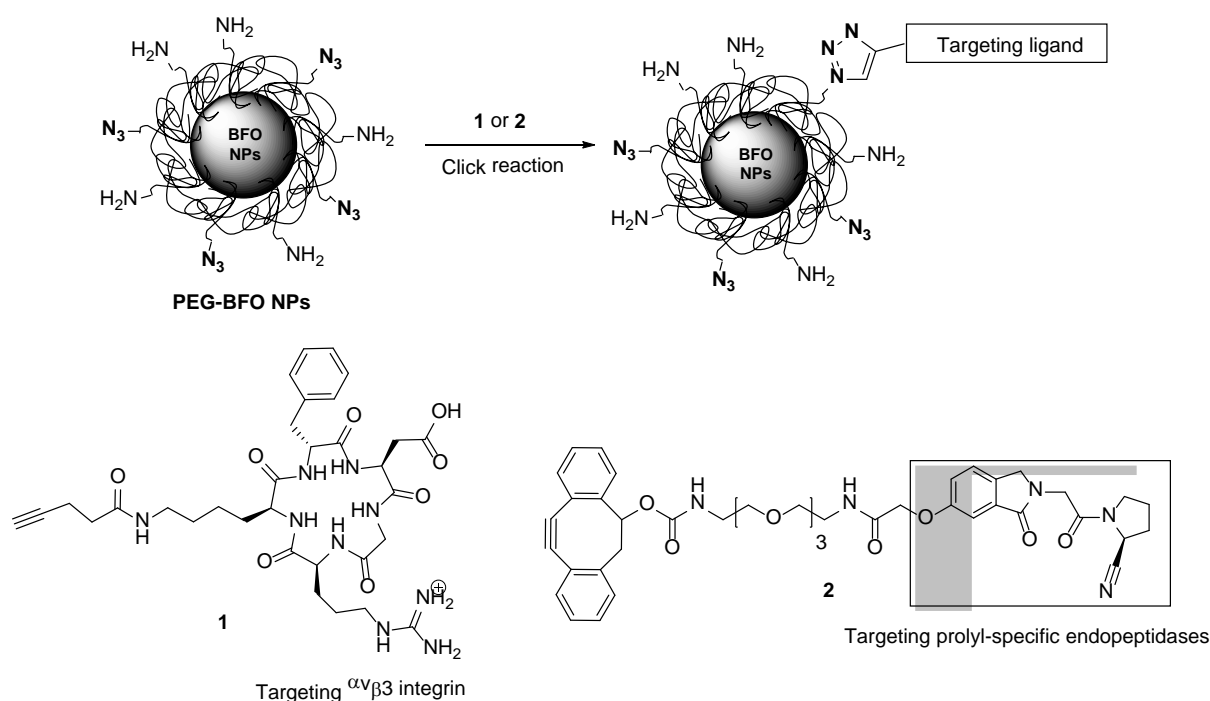
Scheme 1 Functionalization of BFO NPs for cancer cells labeling

Our strategy relies on the conjugation of PEGylated BFO NPs with ligands **1** and **2** as model compounds for the targeting of $\alpha_v\beta_3$ integrin and prolyl-specific endopeptidases expressed by cancer and tumor-associated cells.

Synthesis of targeting ligands for conjugation to harmonic NPs

Ligand **1** resulted from the coupling of cRGDfK, prepared by solid phase peptide synthesis (Borcard et al. 2012), with activated ester of pentynoic acid as previously reported (Passemard et al. 2013). Preparation of ligand **2** started by cleavage of the methyl ether from isoindolinone **3** (prepared according to Powers et al. 2009) followed by subsequent O-alkylation of the corresponding phenol with tert-butyl bromoacetate to afford compound **4** in 45 % yield.

Deprotonation of the lactam moiety followed by condensation with cyano-proline derivative **5** (synthesis described in supporting information) delivered the core of the targeting agent (**6**) in 73% yield. Further derivatization with a cyclooctyne moiety was performed by coupling with compound **7** (synthesis described in supporting information) to provide the targeting ligand **2**, ready to be conjugated to PEGylated BFO NPs. To assess the targeting ability of this ligand toward prolyl-specific endopeptidases in cancer cell lines, functionalization with a biotin label was also performed and delivered compound **8**.
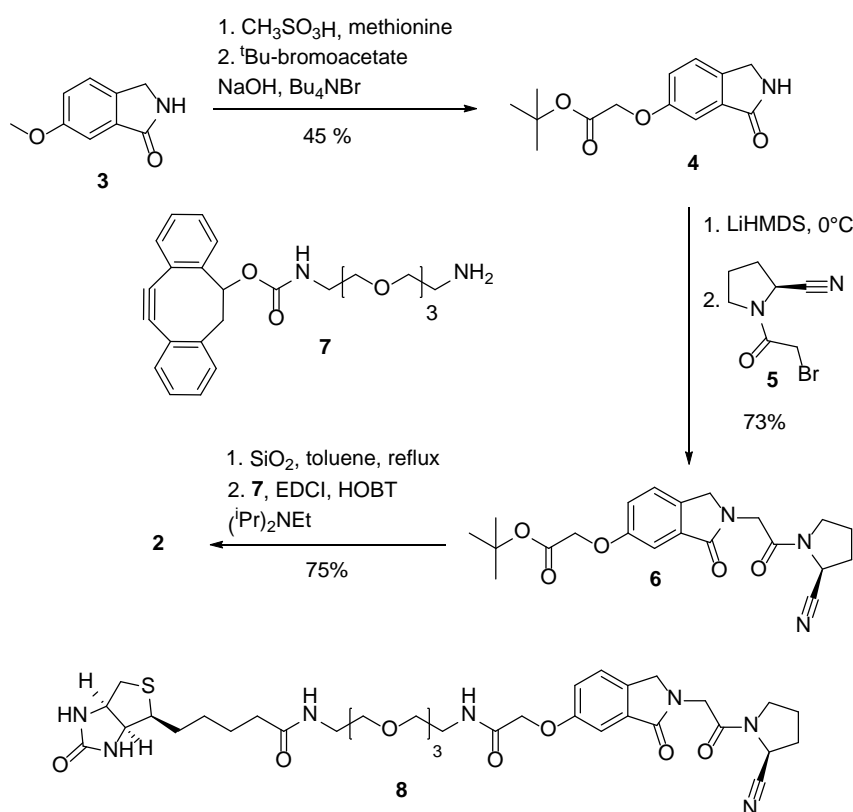

Scheme 2 Synthesis of targeting ligands for further conjugation to harmonic NPs

Functionalization of BFO NPs with targeting ligand **1** and **2**

Starting suspension of BFO NPs (62.5 wt % in ZrO_2 balls, provided by the company FEE (Germany)) was first converted into a stock polydisperse suspension at 3.6 mg/mL (particle size: 128.8 ± 11.2 nm), and then converted into PEGylated nanoparticles (PEG-BFO NPs, particle size: 67.7 ± 5.6 nm), according to a protocol previously described in our group (Staedler et al. 2015) (detailed protocol and characterization is provided in supporting information). Based on recent efforts toward the development of efficient functionalization

pathways for metal oxide NPs (Passemard et al. 2013), PEG-BFO-NPs displaying surface azido and amino functionalities were suspended in distilled water and subjected to [3 + 2]-cycloaddition with ligand **1**, in the presence of copper sulfate and sodium ascorbate (Scheme 3). Ultrasonication for 12 hours followed by removal of copper species by treatment with Cyclam and purification by dialysis afforded BFO NPs conjugated to the ligand targeting $\alpha_v\beta_3$ integrin (**fNP-1**). Alternatively, treatment of PEG-BFO NPs with ligand **2** allowed conjugation by copper-free click reaction to afford **fNP-2**, which were purified by simple washing with toluene to remove unreacted ligand.
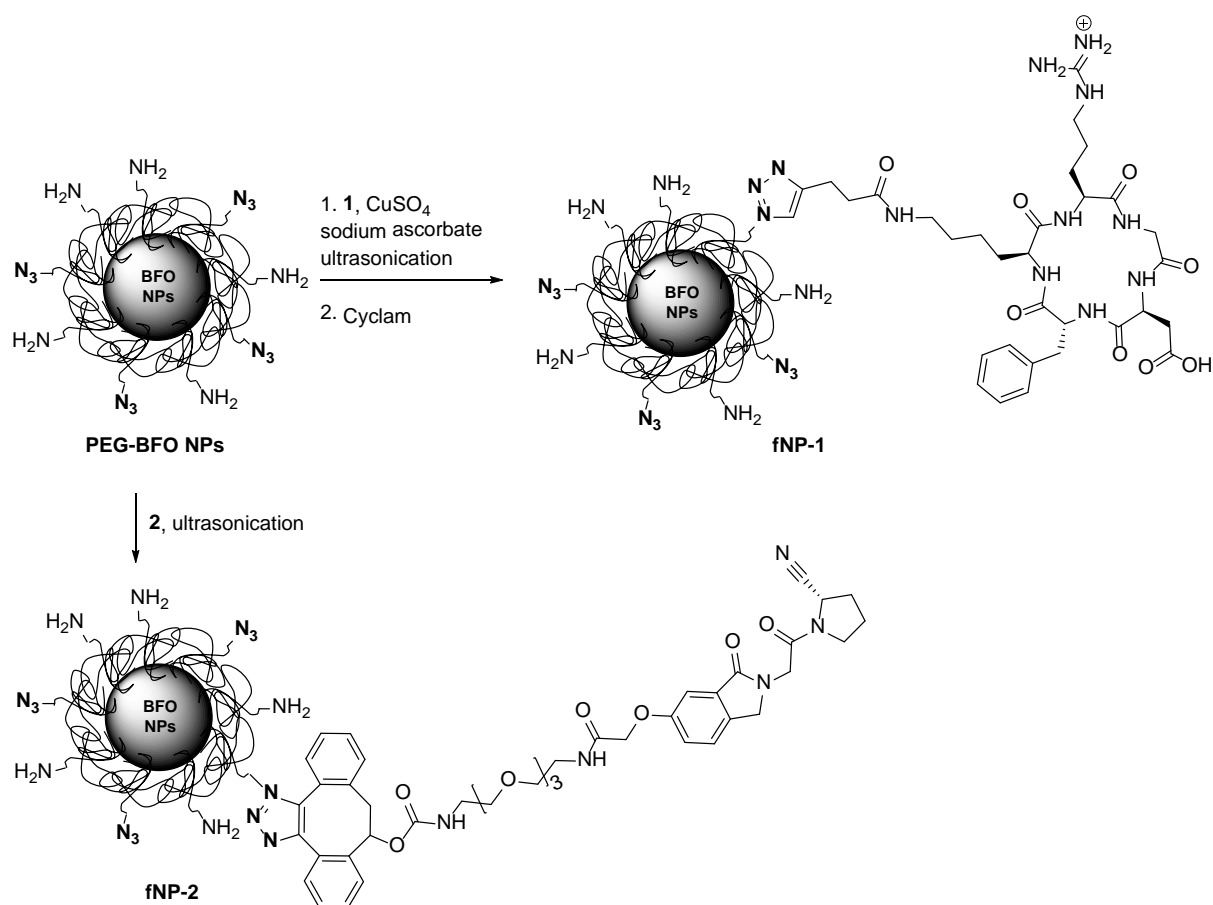
Scheme 3 Functionalization of BFO harmonic NPs by click reaction

Surface functionalization of PEG-BFO NPs was monitored by FT-IR (Figure 1). The formation of the resulting triazole moieties was evidenced by apparition of a C-N stretching band at 1320 (**fNP-1**) and 1390 (**fNP-2**) cm^{-1}. Presence of the peptide ligand in **fNP-1** was indicated by amide stretching bands at 1650 and 1570 cm^{-1}, while nitrile stretching band at 2320 cm^{-1} supported conjugation of targeting ligand **2** to PEG-BFO NPs.
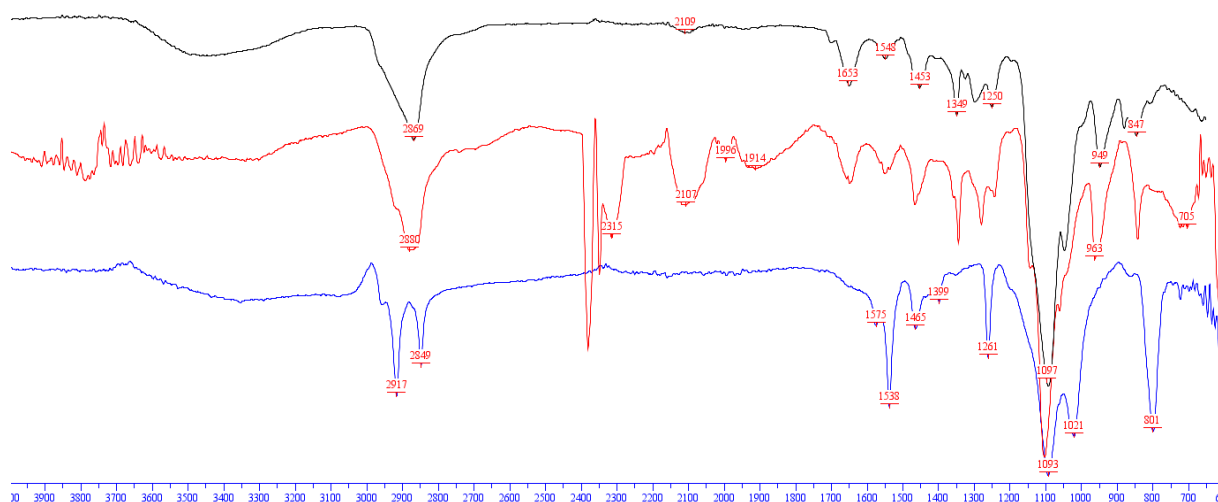
Fig. 1 FT-IR spectra: **PEG-BFO NP** (black), **fNP-1** (red), **fNP-2** (blue)

The coated and functionalized NPs were characterized for their size and surface charge by measurement of the mean hydrodynamic diameter (Dynamic Light Scattering, DLS) and zeta potential (detailed characterization is provided in supporting information). Upon functionalization, the hydrodynamic diameter of harmonic NPs shifted from 67.7 ± 5.6 nm (**PEG-BFO NP**) to 141.8 ± 0 nm for **fNP-1** and to 134.2 ± 11.5 nm for **fNP-2**. The zeta potential value increased from -2.3 ± 0.4 mV (**PEG-BFO NP**) to $+17.3 \pm 0.3$ mV (**fNP-1**) and $+0.7 \pm 0.9$ mV (**fNP-2**).

Targeting ability of functionalized harmonic NPs and cancer cells labelling

The first cellular assays performed with **fNP-1** revealed the presence of traces of residual copper species which resulted in cytotoxic effects on studied cells. Attempts of additional purification were not met with success. Detailed studies were thus carried out on functionalized harmonic nanoparticles **fNP-2**, resulting from copper-free click reaction.

Compound **8** was first assessed for its ability to inhibit prolyl-endopeptidase activity on the most relevant members of the prolyl-oligopeptidase family, both on human recombinant (hr) enzymes and on human lung cancer cells extracts (Table 1). Compound **8** was tested on hrPOP and hrFAPα, as well as on the prolyl exopeptidase dipeptidyl peptidase IV (hrDPPIV) to determine the selectivity toward endo-proteolytic activity.

While compound **8** inhibited both hrFAP-α and hrPOP with Ki values of 0.055 and 0.12 μM, respectively, no significant inhibition was observed for human recombinant DPPIV. This

13

observation suggests the specificity of compound **8** toward oligopeptidases displaying prolyl-endopeptidase activity.

	hrFAPα		hrDPPIV		hrPOP	
	IC$_{50}$ (μM)	K$_i$ (μM)	IC$_{50}$ (μM)	K$_i$ (μM)	IC$_{50}$ (μM)	K$_i$ (μM)
8	0.315	0.055	> 10	-	0.58	0.12

Table 1 Kinetic characteristics for the inhibition of prolyl-oligopeptidases by compound **8** Human recombinant FAP-α (hrFAP-α), DPPIV (hrDPPIV) and POP (hrPOP) were exposed to increasing concentrations (5, 10, 50, 200, 500, 1000, 5000 and 10000 nM) of compound **8**, then to 50 µM of the appropriate substrate (Z-Gly-Pro-AMC for hrFAPα and hrPOP, H-Gly-Pro-AMC for hrDPPIV) and the residual enzymatic activity was determined. The half maximal inhibitory concentration (IC$_{50}$) and the inhibition constant (K$_i$) were calculated.

The inhibition by compound **8** of cell-associated prolyl-endopeptidase activities was then evaluated on a cancer model composed of the three human A549, NCI-H596 and NCI-H520 lung-derived carcinoma cancer cells and the human lung-derived non-tumoral BEAS-2B epithelial cells (Figure 2A). All cancer cells displayed significant enhanced endo-peptidase activity compared to the non-tumoral BEAS-2B cells. Compound **8** inhibited prolyl-endopeptidase activity only in tumor cells and not in the non-tumoral cells, whereas no inhibition of prolyl-exopeptidase activity in these cells was observed (data not shown). In addition, when added to living cells, compound **8** associated with lung-derived A549 cancer cells, but not with non-tumoral BEAS-2B cells (Figure 2B).
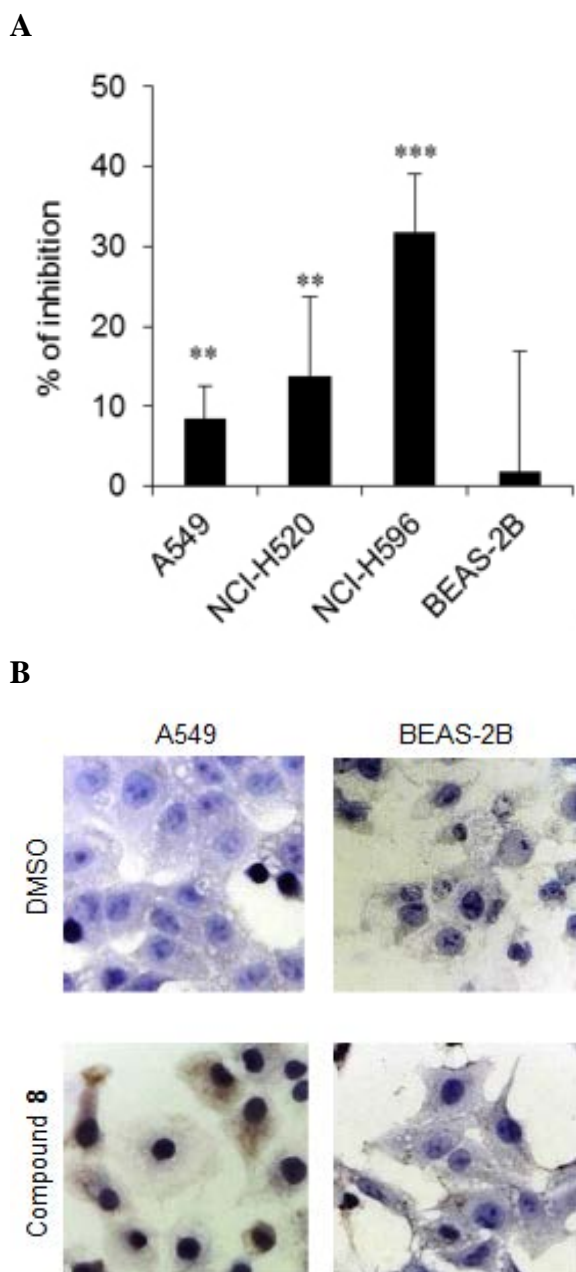
A

B

Fig. 2 Compound **8** inhibits the prolyl-oligopeptidase activity of human lung cancer cells (A) and associates with lung human cancer cells (B)

A. The human lung-derived A549, NCI-H520 and NCI-H596 cancer cells and non-tumoral lung-derived BEAS-2B cells were pre-incubated with 10 µM of compound **8** for 30 min, then the residual enzymatic activity was determined using 50 µM of Z-Gly-Pro-AMC and expressed as percent of inhibition by compound **8**. Exposed cells were compared to cells exposed to solvent (DMSO) using a Student's *t*-test : ** : $p < 0.01$; *** : $p < 0.001$. B. Lung-derived cancer cells (A549) and non-tumoral cells (BEAS-2B) (100'000 cells/well) were exposed to 100 µM compound **8** for 30min, then the association of this compound with the cells was assessed by

adding a peroxidase-conjugated streptavidin. The binding of compound **8** in exposed cells and cells exposed to the vehicle (DMSO) was compared. Blue: counterstain with haematoxylin; brown spots: compound 3 detected by streptavidin. Magnification: 400x.

Based on these results, the targeted labelling of human lung cancer cells with **fNP-2** was investigated using one tumoral (NCI-H520) and one non-tumoral (BEAS-2B) lines. PEGylated harmonic NPs (**PEG-BFO NPs**) were considered as negative controls. The cells were exposed to **fNP-2**, then labelled with a fluorescent probe for cell membranes, and the harmonic NPs were revealed by detecting their SHG signal (excitation at 790 nm) (Figure 3).
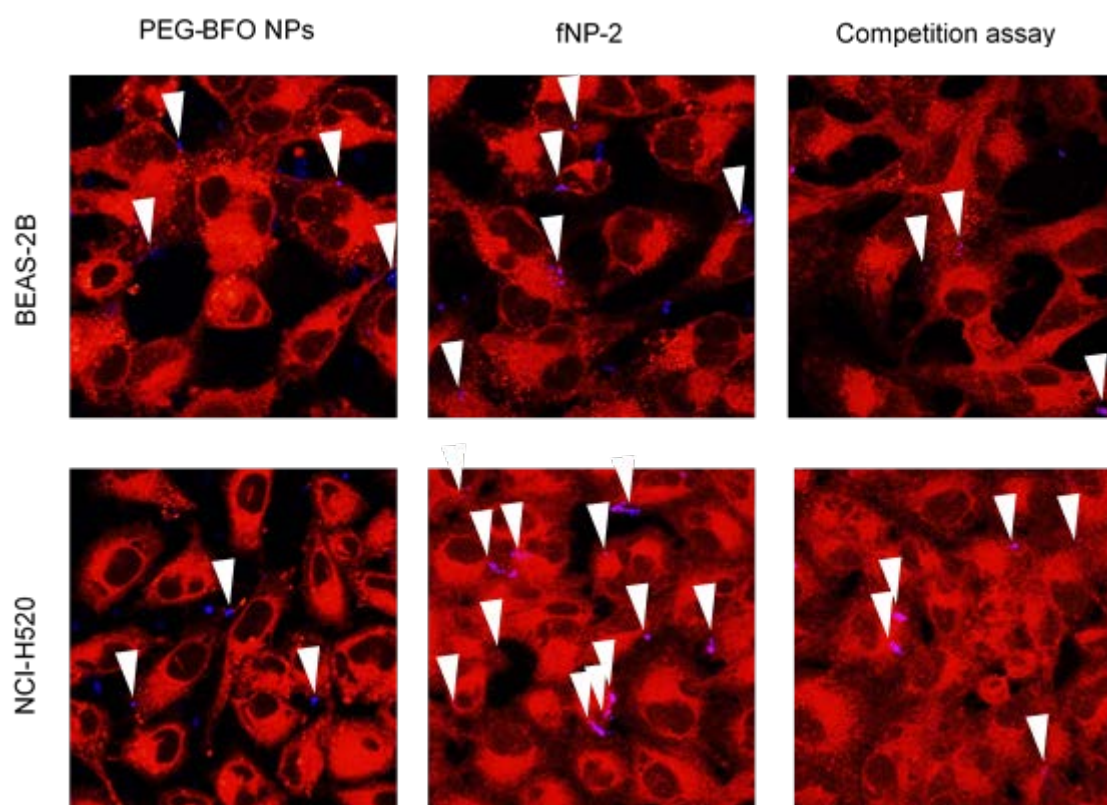

Fig. 3 Cancer cells labelling using **fNP-2**

Lung-derived NCI-H520 (tumoral) and BEAS-2B (non-tumoral) cells (100'000 cells/well) were exposed for 30 min to 50 µg/mL of **PEG-BFO NP**, to 50 µg/mL of **fNP-2** or to 50 µg/mL of **fNP-2** after 30min pre-incubation with 100 µM of compound **8** (Competition assay), then the cells were fixed and the cell membranes were labelled using the fluorescent probe FM1-43FX (red). SHG of NPs was detected by multiphoton microscopy (blue, those associated with cells are indicated with white arrows). Magnification: 200x.

In order to evaluate the specificity of the targeting, a competition assay was done, in which lung-derived NCI-H520 cancer cells were incubated with compound **8** alone prior to being exposed to **fNP-2**. Cells labelled with NPs were counted and the number of cells displaying association with the NPs was expressed as the percent ratio of positive cells to total cells in a microscopic field (Figure 4).
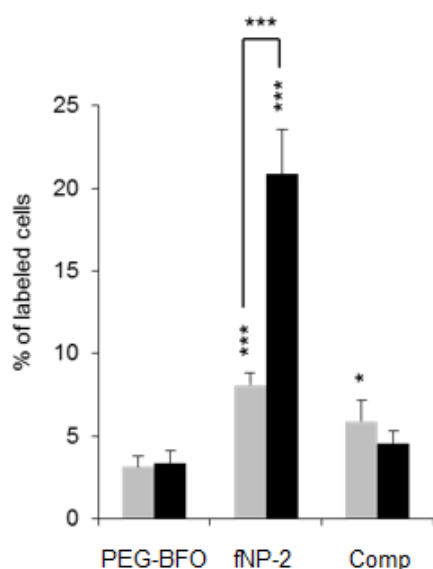

Fig. 4 Quantification of cells labelled with **fNP-2**

Human lung-derived NCI-H520 (tumoral, black bars) and BEAS-2B (non-tumoral, grey bars) cells were exposed to 25 µg/mL of **PEG-BFO NP**, to 50 µg/mL of **fNP-2** or to 25 µg/mL of **fNP-2** after 30 min pre-incubation with 100 µM of compound **8** (Comp). The number of labelled cells was expressed as the percent of the ratio of cells displaying association with the NPs to the total cells in a microscopy field (magnification 200x). The percentages of cells labelled with **PEG-BFO NP** were compared to those of cells labelled with **fNP-2**, then tumoral cells were compared to non-tumoral cells using a Student's t-test : *$p<0.05$; ***$p < 0.001$.

Both cancer cells and non-tumoral cells were labelled with **fNP-2**, but the number of cancer cells associated with **fNP-2** was significantly much higher than for non-tumoral cells. Moreover, in the competition assay the quantification of the association clearly revealed that the binding was target-specific. These results suggest that harmonic BFO NPs can be efficiently transformed into labeling nanodevices targeting proteins expressed at the surface of cancer cells.

Conclusion

Here we present a general approach for the functionalization of imaging NPs with low molecular weight tumor-specific targeting agents. In particular, copper-free click reaction allows highly efficient conjugation of alkynyl containing ligands to PEGylated BFO NPs displaying surface reactive azido groups. The resulting nanoparticles combine imaging properties and specific recognition of cancer cell biomarkers offering new modalities for improved early cancer diagnosis, a presently unmet need (Zuo et al. 2007). Following the demonstration of the potential of BFO-NPs for bio-imaging and selective photointeraction (Staedler et al. 2014) and the study of their biological effect (Staedler et al. 2015), the present study demonstrate, for the first time, their ability to be converted into targeted imaging nanodevices. While the selectivity factor for the labelling of cancer cells vs non-tumoral cells need to be improved, the strategy illustrated herein can be easily transferred to other metal oxide NPs, thus enlarging the range of detection modalities. In addition, the use of a specific covalent inhibitor of cell membrane prolyl endo-peptidases that can be further modified without affecting its affinity for the targeted enzymes, appears as an appealing methodology for targeting cancer and tumor-associated cells.

Acknowledgments

References

Ahmad P, Khandaker MU, Amin YM, Khan ZR (2015) Synthesis of boron nitride microtubes and formation of boron nitride nanosheets. Materials and Manufacturing Processes 30(2) 184-188. doi: 10.1080/10426914.2014.952041

Arruebo M, Valladares M, Gonzalez-Fernadez A (2009) Antibody-conjugated nanoparticles for biomedical applications. J. Nanomater. Article ID 439389. doi:10.1155/2009/439389

Bardhan R, Lal S, Joshi A, Halas NJ (2011) Theranostic nanoshells: from probe design to imaging and treatment of cancer. Acc. Chem. Res. 44(10): 936-946. doi: 10.1021/ar200023x

Baumner R, Bonacina L, Enderlein J, Extermann J, Fricke-Begemann T, Marowsky G, Wolf JP (2010) Evanescent-field-induced second harmonic generation by noncentrosymmetric nanoparticles. Opt. Express 18(22): 23218-23225. doi: 10.1364/OE.18.023218

Bonacina L (2012) Nonlinear nanomedicine: harmonic nanoparticles toward targeted diagnosis and therapy. Mol. Pharmaceutics 10(3): 783-792. doi: 10.1021/mp300523e

Borcard F, Staedler D, Comas H, Juillerat FK, Sturzenegger PN, Heuberger R, Gonzenbach UT, Juillerat-Jeanneret L, Gerber-Lemaire S (2012) Chemical functionalization of bio-ceramics to enhance endothelial cells adhesion for tissue engineering. J Med Chem 55:7988-7997. doi: 10.1021/jm301092r

Brennen WN, Isaacs JT, Denmeade SR (2012) Rationale behind targeting fibroblast activation protein-expressing carcinoma-associated fibroblasts as a novel chemotherapeutic strategy. Mol Cancer Ther 11: 257-266. doi: 10.1158/1535-7163.MCT-11-0340

Cer RZ, Mudunuri U, Stephens R, Lebeda FJ (2009) IC50-to-Ki: a web-based tool for converting IC50 to Ki values for inhibitors of enzyme activity and ligand binding. Nucleic Acid Res. 37:W441-445. doi: 10.1093/nar/gkp253

Chinen AB, Guan CM, Ferrer JR, Barnaby SN, Merkel TJ, Mirkin CA (ASAP) Nanoparticle Probes for the Detection of Cancer Biomarkers, Cells, and Tissues by Fluorescence. Chem. Rev. doi: 10.1021/acs.chemrev.5b00321

Cohen BE (2010) Biological imaging: beyond fluorescence. Nature 467:407-408. doi:10.1038/467407a

Čulić-Viskota J, Dempsey WP, Fraser SE, Pantazis P (2012) Surface functionalization of barium titanate SHG nanoprobes for in vivo imaging in zebrafish. Nat. Protoc. 7: 1590-1607. doi:10.1038/nprot.2012.081

Danhier F, Le Breton A, Préat V (2012) RGD-based strategies to target alpha(v)beta(3) integrin in cancer therapy and diagnosis. Mol. Pharmaceutics 9: 2961-2973. doi: 10.1021/mp3002733

Dempsey WP, Fraser SE, Pantazis P (2012) SHG nanoprobes: advancing harmonic imaging in biology. Bioesssays 34: 351-360. doi: 10.1002/bies.201100106

Desgrosellier JS, Cheresh DA (2010) Integrins in cancer: biological implications and therapeutic opportunities. Nat. Rev. Cancer 10(1): 9-22. doi: 10.1038/nrc2748

Erathodiyil N, Ying JY (2011) Functionalization of inorganic nanoparticles for bioimaging applications. Acc. Chem. Res. 44(10): 925-935. doi: 10.1021/ar2000327

Extermann J, Bonacina L, Cuña E, Kasparian C, Mugnier Y, Feurer T, Wolf, JP (2009) Nanodoublers as deep imaging markers for multiphoton microscopy. Opt. Express 17(17): 15342-15349. doi: 10.1364/OE.17.015342

Hsieh CL, Grange R, Pu Y, Psaltis D (2010) Three-dimensional harmonic holographic microscopy using nanoparticles as probes for cell imaging: erratum. Opt. Express 18(4): 3456-3457. doi: 10.1364/OE.18.003456

Hsieh CL, Pu Y, Grange R, Laporte G, Psaltis D (2010) Imaging through turbid layers by scanning the phase conjugated second harmonic radiation from a nanoparticle. Opt. Express 18(20): 20723-20731. doi: 10.1364/OE.18.020723

Juillerat-Jeanneret L, Gerber-Lemaire S (2009) The prolyl-aminodipeptidases and their inhibitors as therapeutic targets for fibrogenic disorders. Mini Rev Med Chem 9(2): 215-226. doi:10.2174/138955709787316100

Kairdolf BA, Smith AM, Stokes TH, Wang MD, Young AN, Nie S (2013) Semiconductor quantum dots for bioimaging and biodiagnostic applications. Annu. Rev. Anal. Chem. 6:143-162. doi: 10.1146/annurev-anchem-060908-155136

Lawandi J, Gerber-Lemaire S, Juillerat-Jeanneret L, Moitessier N (2010) Inhibitors of prolyl oligopeptidases for the therapy of human diseases: defining diseases and inhibitors. J. Med. Chem. 53: 3423-3438. doi: 10.1021/jm901104g

Le Xuan L, Zhou C, Slablab A, Chauvat D, Tard C, Perruchas S, Gacoin T, Villeval P, Roch JF (2008) Photostable second-harmonic generation form a single KTiOPO$_4$ nanocrystal for nonlinear microscopy. Small 4: 1332-1336. doi: 10.1002/smll.200701093

Magouroux T, Extermann J, Hoffmann P, Mugnier Y, Le Dantec R, Jaconi ME, Kasparian C, Ciepielewski D, Bonacina L, Wolf JP (2012) High-speed tracking of murine cardiac stem cells by harmonic nanodoublers. Small 8: 2752-2756. doi: 10.1002/smll.201200366

Meyer T, Schmitt M, Dietzek B, Popp J (2013) Accumulating advantages, reducing limitations: multimodal nonlinear imaging in biomedical sciences – The synergy of multiple contrast mechanisms. J. Biophoton. 6: 887–904. doi: 10.1002/jbio.201300176

Pantazis P, Maloney J, Wu D, Fraser SE (2010) Second harmonic generation (SHG) nanoprobes for in vivo imaging. Proc. Natl. Acad. Sci. U.S.A. 107(33): 14535-14540. doi: 10.1073/pnas.1004748107

Passemard S, Staedler D, Ucnova L, Schneiter GS, Kong P, Bonacina L, Gerber-Lemaire S (2013) Convenient synthesis of heterobifunctional poly(ethylene glycol) suitable for the functionalization of iron oxide nanoparticles for biomedical applications. Bioorg Med Chem 23: 5006-5010. doi:10.1016/j.bmcl.2013.06.037

Poplawski S., Lai JH, Li Y, Jin Z, Liu Y, Wu W, Wu Y, Zhou Y, Sudmeier JL, Sanford DG, Bachovchin WW (2013) Identification of selective and potent inhibitors of fibroblast activation protein and prolyl oligopeptidase. J. Med. Chem. 56:3467-3477. doi: 10.1021/jm400351a

Powers JJ, Favor DA, Rankin T, Sharma R, Pandit C, Jeganathan A, Maiti SN (2009) Synthesis of methyl-, fluoro-, and chloro-substituted 6-hydroxyisoindolin-1-ones. Tetrahedron Lett. 50:1267-1269. doi: 10.1016/j.tetlet.2008.12.099

Rostovtsev VV, Green LG, Fokin VV, Sharpless KB (2002), A Stepwise Huisgen Cycloaddition Process: Copper(I)-Catalyzed Regioselective "Ligation" of Azides and Terminal Alkynes. Angew. Chem. Int. Ed., 41: 2596–2599. doi: 10.1002/1521-3773(20020715)41:14<2596::AID-ANIE2596>3.0.CO;2-4

Schwung S, Rogov A, Clarke G, Joulaud C, Magouroux T, Staedler D, Passemard S, Jüstel T, Badie L, Galez C, Wolf JP, Volkov Y, Prina-Mello A, Gerber-Lemaire S, Rytz D, Mugnier Y, Bonacina L, Le Dantec R (2014) Nonlinear optical and magnetic properties of BiFeO3 harmonic nanoparticles. J. Appl. Phys. 116: 114306. doi: 10.1063/1.4895836

Sletten EM, Bertozzi CR (2011) From mechanism to mouse: a tale of two biorthogonal reactions. Acc. Chem. Res. 44(9): 666-676. doi: 10.1021/ar200148z

Staedler D, Magouroux T, Hadji R, Jouloud C, Extermann J, Schwung S, Passemard S, Kasparian C, Clarke G, Gerrmann M, Le Dantec R, Mugnier Y, Rytz D, Ciepielewski D, Galez C, Gerber-Lemaire S, Juillerat-Jeanneret L, Bonacina L, Wolf JP (2012) Harmonic Nanocrystals for Bio-Labeling: a Survey of Optical Properties and Biocompatibility. ACS Nano 6, 2542-2549. doi: 10.1021/nn204990n

Staedler D, Magouroux T, Passemard S, Schwung S, Dubled M, Schneiter GS, Rytz D, Gerber-Lemaire S, Bonacina L, Wolf JP (2014) Deep UV Generation and Direct DNA Photo-Interaction by Harmonic Nanoparticles in Labelled Samples. Nanoscale 6:2929-2936. doi:10.1039/c3nr05897b

Staedler D, Passemard S, Magouroux T, Rogov A, Maguire CM, Mohamed BM, Schwung S, Rytz D, Jüstel T, Hwu S, Mugnier Y, Le Dantec R, Volkov Y, Gerber-Lemaire S, Prina-Mello

A, Bonacina L, Wolf JP (2015) Cellular uptake and biocompatibility of bismuth ferrite harmonic advanced nanoparticles. Nanomedicine: NBM 11: 815-824. doi:10.1016/j.nano.2014.12.018

Sun C, Sze R, Zhang MQ (2006) Folic acid-PEG conjugated superparamagnetic nanoparticles for targeted cellular uptake and detection by MRI. J. Biomed. Mater. Res. A 78A: 550-557. doi: 10.1002/jbm.a.30781

Wang Y, Gu H (2015) Core-shell-type magnetic mesoporous silica nanocomposites for bioimaging and therapeutic agent delivery. Adv. Mater. 27: 576-585. doi: 10.1002/adma.201401124

Wen J, Xu Y, Li H, Lu A, Sun S (2015) Recent applications of carbon nanomaterials in fluorescence biosensing and bioimaging. Chem. Commun. 51: 11346-11358. doi: 10.1039/c5cc02887f

Wolfbeis OS (2015) An overview of nanoparticles commonly used in fluorescent bioimaging. Chem. Soc. Rev. 44: 4743-4768. doi: 10.1039/c4cs00392f

Yao J, Yang M, Duan Y (2014) Chemistry, biology and medicine of fluorescent nanomaterials and related systems: new insights into biosensing, bioimaging, genomics, diagnostics and therapy. Chem. Rev. 114: 6130-6178. doi: 10.1021/cr200359p

Zhou J, Liu Q, Feng W, Sun Y, Li F (2015) Upconversion luminescent materials: advances and applications. Chem. Rev. 115(1): 395-465. doi: 10.1021/cr400478f

Zuo L, Wei WC, Morris M, Wei JC, Gorbounov M, Wei CM (2007) New technology and clinical applications of nanomedicine. Med. Clin. N. Am. 91:845-862.